Contents lists available at ScienceDirect

Arabian Journal of Chemistry

journal homepage: www.ksu.edu.sa

Near-infrared light and pH-responsive hyaluronic acid-enveloped ZIF-8 nanoparticles for the treatment of pneumonia caused by methicillin-resistant *Staphylococcus aureus*

Yujie Xu [b], Xiaoli Zhang [c], Shuyi Liang [a], Congmin Niu [a], Jiayi Guo [a], Chunbo Lu [a,*]

[a] *Weifang Med Univ, Sch Biosci & Technol, Key Lab Biol Med Univ Shandong Prov, Baotong Rd, Weifang 261053, Shangdong, China*
[b] *College of Chemistry & Pharmacy, Shaanxi Key Laboratory of Natural Products & Chemical Biology, Northwest A&F University, Yangling 712100, Shaanxi, China*
[c] *The 80th Group Army Hospital of Chinese People' Liberation Army, Weifang 261053, Shangdong, China*

ARTICLE INFO

Keywords:
Hyaluronic acid
Zeolitic imidazolate framework-8
Nanoplatform
Multidrug-resistant bacterial
Photodynamic sterilization

ABSTRACT

There is a serious threat to public health posed by the rapid spread of methicillin-resistant *Staphylococcus aureus* (MRSA). Photodynamic sterilization is the most effective method of combating bacterial infection, especially multidrug-resistant bacterial infection. In this study, zeolitic imidazolate framework-8 (ZIF-8) nanoparticles, one of the most attractive metal–organic framework material, were used to encapsulate the indocyanine green (ICG, a potent PS); after that, hyaluronic acid (HA) coating was applied to the nanoparticle to create a host cell-tracking nanoplatform (ICG@ZIF-8/HA). Upon near-infrared light irradiation, ICG@ZIF-8/HA exhibit excellent efficacy in producing reactive oxygen species (ROS) and killing multidrug-resistant bacteria *in vitro*. After the tail vein injection, ICG@ZIF-8/HA can precisely deliver to lung infection sites, and display an effective PDT-based elimination of multidrug-resistant bacteria in mouse lung infection models. These results suggest that the ICG@ZIF-8/HA nanoplatform may exhibit potent curative effects on infectious diseases.

1. Introduction

In recent years, Methicillin-resistant *Staphylococcus aureus* (MRSA), which is widely known as a Gram-positive pathogen, has become an urgent threat to human health around the world (Gerlach et al., 2018; Tong et al., 2015; Hennekinne et al., 2021). Pneumonia caused by MRSA is higher mortality rate than other pathogens because it tends to infect patients with multiple complications. MRSA isolates in clinical settings are resistant not only to lactams, but also to vancomycin, linezolid, and other relatively new antibiotics such as daptomycin (Gajdács, 2019; Nannini et al., 2010). Unfortunately, infections caused by *Staphylococcus aureus* in nosocomial settings are on the rise, which means that there are fewer options available for treating them (Rehm, 2008). MRSA's sustained emergence and rapid spread, together with the lack of new antibiotics, suggest a post-antibiotic era and an urgent need for novel antimicrobial agents (Gardete and Tomasz, 2014; McGuinness et al., 2017; Stogios and Savchenko, 2020).

Recently, there have been growing numbers of antibacterial agents developed for eliminating MRSA, such as antibody conjugated with antibiotic (Lehar et al., 2015), quaternary ammonium compounds (Żywicka et al., 2018), cationic polymers (Hou et al., 2017), photothermal therapy (PTT) or photodynamic therapy (PDT) (Yuwen et al., 2021; Hu et al., 2020; Chang et al., 2021) and so on. The PDT approach, which exhibits advantages such as minimal invasion and bare drug resistance, has been gaining increasing interest as an emerging strategy to treat MRSA (Pérez et al., 2021; Zhang et al., 2022). When irradiated with a certain wavelength of light, photosensitizers (PS) absorb light energy and produce cytotoxic reactive oxygen species (ROS) to kill bacteria (Ribeiro et al., 2022). To achieve efficient PDT, PS must be delivered to the infection site in a targeted and effective manner. However, in practice, a lot of PS is used in PDT with low tissue selectivity, poor solubility in water, and low transfer efficiency (Zhao et al., 2019; Li et al., 2017). As a result, the development of a nanoplatform that delivers PS to infection sites effectively will enhance the efficacy of PDT.

As a class of nanomaterial with high porosity, biocompatibility, and tunable functionality, metal organic frameworks (MOFs) are gaining traction in drug delivery applications (Yan et al., 2023; Zhao et al., 2022;

Peer review under responsibility of King Saud University.
* Corresponding author.
E-mail address: lucb163@163.com (C. Lu).

https://doi.org/10.1016/j.arabjc.2023.105426
Received 10 April 2023; Accepted 1 November 2023
Available online 2 November 2023

Zhang et al., 2022). The zeolitic imidazolate framework-8 (ZIF-8) is the most promising of these MOFs as an attractive nanocarrier for the delivery of functional molecules and the delivery of good drug payloads (Gao et al., 2019). According to reports, strong acid conditions can disintegrate ZIF-8 instantly, while slightly acidic environments degrade it slowly (Tian et al., 2021; Zhang et al., 2019). Due to the slightly acidic environment of infected tissue, ZIF-8 is an excellent drug delivery system.

A natural polysaccharide, hyaluronic acid (HA) has good hydrophilic and biodegradable properties (Thompson et al., 2018). As HA combines with CD44 that are usually excessively overexpressed on the surface of many types of macrophage, it increases the accumulation in the infection site and can actively target immune cells (McDonald and Kubes, 2017). As well, HA chains can be disintegrated by hyaluronidase (HAase), which is abundant in the so-called infection microenvironment (Yao et al., 2017), thus exposing wrapped PS for bacterial infection treatment.

Herein, we present a simple but versatile method for improving indocyanine green's (ICG, a potent PS) poor stability and low tissue selectivity by encapsulating it in ZIF-8 compounds (defined as ICG@ZIF-8). Then, the ICG@ZIF-8/HA (abbreviated to IZH) nanoplatform is formed by electrostatic interaction with an HA shell as a smart "switch" and an infection site targeted "guider". In the first place, the active targeting interaction between HA and immune cells overexpressing HA receptors allowed IZH to effectively target infection sites. Subsequently, the IZH was degraded in the microenvironment of acid infection and released the encapsulated ICG. By irradiating lasers, cytotoxic ROS are produced, which can kill MRSA. *In vitro* and *in vivo* experiments showed that the IZH nanoplatform significantly affected MRSA infection treatment, providing an innovative treatment for pneumonia caused by methicillin-resistant *Staphylococcus aureus*.

2. Materials and methods

2.1. Materials

Hyaluronic acid (~ 10 kDa), purchased from QuFu GuangLong Biochem Co., Ltd. 2-Methylimidazole, zinc nitrate hexahydrate ($Zn(NO_3)_2{\cdot}6H_2O$), Indocyanine green (ICG) were purchased from Aladdin. Fluorescein isothiocyanate (FITC), 4′,6-Diamidino-2-phenylindole (DAPI), 3-(4, 5-dimethylthiazol-2-yl)-2, 5-diphenyl tetrazolium bromide (MTT), Degradation of 1,3-diphenyl-isobenzofuran (DPBF) were purchased from Sigma Co. (St. Louis, MO, USA). Analytical-grade chemicals and solvents were used without further purification.

Prof. Wang (College of Life Sciences, Northwest A&F University) generously donated *Staphylococcus aureus* (MRSA) and Macrophages (RAW264.7). We obtained Kunming mice from Pengyue Experimental Animal Breeding (Jinan, China).

2.2. Synthesis of IZH

Synthesis of IZH was performed using the one-pot encapsulation method with a few modifications based on previous literature descriptions (Xie et al., 2019). Specifically, 2 mL of 2-methylimidazole (2-MIM, 2.78 M) aqueous solution was added to 200 μL of ICG (10 mg/mL in DMSO) under gentle stirring at 400 rpm for 15 min at 25 °C. Then, 15 min were needed to stir the reaction mixture after 160 μL of zinc nitrate aqueous solution (0.48 M) was dropped in dropwise. Centrifugation (12,000 rpm, 25 min at 4 °C) was used to collect ICG@ZIF-8, which was then washed three times with H_2O and re-dispersed in 2 mL of H_2O. After aging for 30 min, 2 mL HA aqueous solution (2 mg /mL) was added and the mixture was aged in the dark for 30 min. Finally, the product was collected by centrifugation. According to the equation below, DLC can be defined as follows:

$$\mathrm{DLC}(\%) = \frac{\text{The amount of loaded drug}}{\text{Total amount of nanocarriers and loaded drug}} \times 100$$

To determine the loaded efficiency of ICG, an acidic aqueous solution was used to dissolve the IZH powder and measured at a wavelength of 780 nm according to UV–vis characteristic absorption peak.

2.3. Characterization of IZH

Scanning electron microscopy (SEM-450field emission, FEI, Hillsboro) was used to investigate the morphology of nanoparticles.

The UV–vis spectra measurement was conducted on a UV–vis spectrophotometer (Thermo Evolution 300 spectrophotometer).

The FTIR spectra were detected using an FTIR spectrometer (BRUKER TEMSOR 27, Germany).

The particle size and zeta potential were measured by a Zetasizer Nano ZS (Malvern, U.K.). In addition, the zeta potential and particle size of IZH NPs stored at 4 °C were assessed over a predetermined period (0, 0.5, 1, 2, 3, 4, 5 and 6 days) to assess their stability.

2.4. In vitro release of ICG from IZH

IZH was incubated at 37 °C with buffer solutions of pH 5.5 and 7.4 to determine *in vitro* ICG release. Under shaking, nanoparticles were placed in 5 mL of buffer solution to investigate ICG release from IZH. At regular time intervals, the diffusion medium was taken and supplemented with fresh buffer solution in the same amount. ICG drug release from samples was measured using a UV–vis spectrometer. There were three tests on all samples.

2.5. ROS generation detection

A reactive oxygen quencher (Wang et al., 2019), 1,3-diphenyl-isobenzofuran (DPBF), was studied with IZH. Free ICG and IZH containing the same amount of ICG were added with DPBF (20 μg/mL). Then, NIR lasers of 780 nm were used (2 W/cm^2) to illuminate the mixture. At regular time intervals, a UV–vis spectrophotometer was used to measure the absorption spectra of DPBF.

2.6. Biocompatibility analysis

During this experiment, nanoparticles were examined for their toxicity to cells. Firstly, RAW 264.7 cells were cultivated at 37 °C in 96-well plates with 5 % CO_2. Then, the final IZH composite was diluted and added to the tested wells at various concentrations. A standard 3-(4, 5-dimethylthiazol-2-yl)-2, 5 di-phenyltetrazolium bromide (MTT) assay was used to assess cell viability.

As previously reported (Lu et al., 2020), the hemolysis assay was performed with IZH to check its compatibility with blood. In brief, red blood cells (RBC) solution (2 % w/w) of 0.1 mL was added to 1.9 mL of the solution of IZH (200 μg/mL). Thereafter, the specimens were continuously incubated at 37 °C for 1 h. In the following step, centrifugation at 6500 rpm for 10 min was carried out on the obtained mixtures. Finally, an automated microplate reader was used to determine the absorbance of the centrifuged supernatant at 545 nm. Among the control groups, PBS served as a negative control group and pure water served as a positive control group.

$$Hemolysisratio(\%) = \left(OD_{sample} - OD_{negative}\right) / \left(OD_{positive} - OD_{negative}\right) \times 100$$

2.7. Cellular uptake of IZH

The uptake efficiency of IZH by Immune cells was evaluated by using RAW 246.7 cells. The cells were seeded in 6-well plates cell culture dishes overnight. Then, excess free HA (3 mg/mL) was added to a group

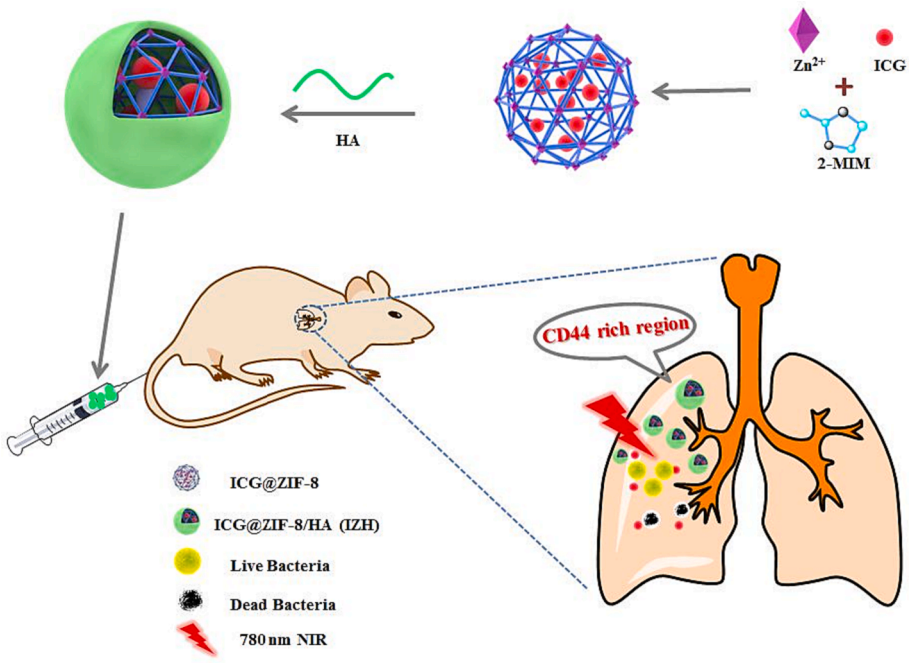

Fig. 1. A schematic illustration showing ICG@ZIF-8/HA nanoplatform targeted at the infected site.

of cells and incubated for 2 h. The medium was then replaced with a fresh medium containing FITC-loaded IZH (50 μg/mL) and continued cultivating for 3 h. Finally, DAPI was used to stain the cells after several rinses with PBS. Cells were observed using a fluorescence microscope (Olympus BX53).

2.8. Intracellular bacteria experiment

For the construction of infected cells, MRSA were co-incubated with RAW 264.7 cells for 1 h in a cell culture medium. Gentamicin was then added at 50 μg/mL to inhibit extracellular bacterial growth. After adding the test material and control material to the culture medium, the medium was incubated at 37 °C for further 12 h. RAW 264.7 cells were serially diluted with PBS supplemented with TritonX-100. In order to calculate colony-forming units (CFU), live bacterial numbers were plated and their numbers were determined.

2.9. In vivo activity evaluation

As a model for bacterial pneumonia in mice, the following procedures were used: briefly, after isoflurane anesthesia (1.5–2.5 %) was administered, mice were then infected with MRSA (10 μL, 10^9 CFU/mL) through weasand. Infected mice were divided into five groups: (5 mice per group) randomly: (a) PBS; (b) ZIF-8@HA; (c) IZH; (d) ICG with laser; (e) IZH with laser. For therapeutic evaluation, PBS, ZIF-8/HA, ICG and IZH (5 mg/kg) were intravenously injected via the tail vein into mice for five days. Following administration, NIR laser (780 nm, 2 W/cm^2) illumination of the mice's chest was performed for 6 min, with 2 min

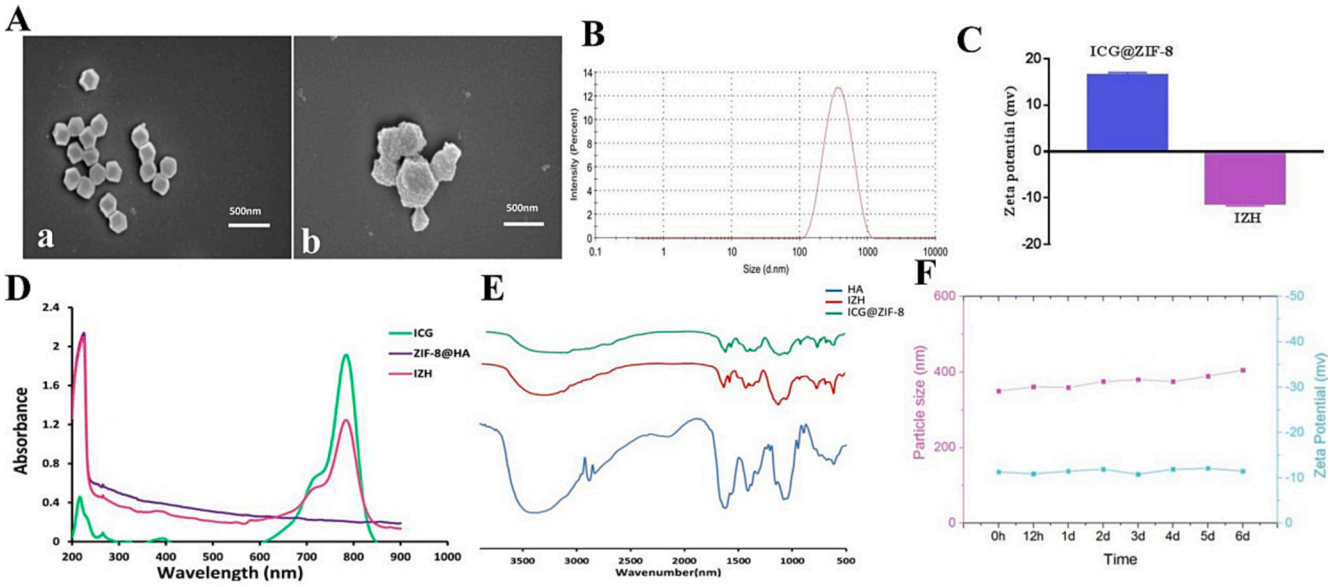

Fig. 2. (A) SEM images of ICG@ZIF-8 (a) and IZH (b), (B) Distribution curve of IZH particle sizes; (C) Zeta potential of ICG@ZIF-8 and IZH (D) UV–vis spectra;(E) FT-IR spectra. (F) An analysis of changes in particle size and zeta potential of IZH after 6 days of storage.

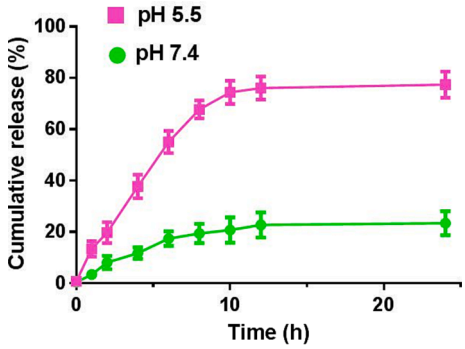

Fig. 3. *In vitro* drug release behaviors of IZH under different pH conditions.

between each spot of laser exposure. At the end of the experiment, further analysis was performed on the lungs collected separately. Counts of bacteria were calculated for each organ as before. Additionally, lung tissue structure showed changes by hematoxylin and eosin (H&E) staining.

2.10. Statistical analysis

Experimental data were presented as mean ± standard deviation (SD) and plotted and statistical analysis was determined using the software GraphPad Prism 7.01.

3. Results and discussion

3.1. Synthesis and characterization

As shown in Fig. 1, through a simple one-pot biomineralizing method, ICG@ZIF-8 nanoparticles (NPs) were synthesized successfully. In order to improve targeting capability, HA shell was deposited on the surface of ICG@ZIF-8 via coordination bonds. By scanning electron microscope (SEM), ICG@ZIF-8 and IZH were measured in terms of size and morphology. As illustrated in Fig. 2A, the ICG@ZIF-8 NPs have a uniform diameter of about 250 nm and are monodispersed. Compared with ICG@ZIF-8 NPs, IZH NPs display rougher three-dimensional structures and obvious shell structures, which demonstrate that HA was successfully coated and IZH NPs were successfully synthesized. As indicated in Fig. 2B, DLS has determined that the average diameter of IZH NPs is approximately 375 nm. Generally, ICG@ZIF-8 is known to have a positive surface charge because of the exposed metal components (Zn^{2+}) on the external surface. A significant change in zeta potential was observed after HA-modification from + 16.38 mV to −11.28 mV in inverse proportion (Fig. 2C), because HA contains many carboxyl groups which are negatively charged.

As shown in Fig. 2D, compared to those of pure ZIF-8@HA, both ICG and IZH demonstrated characteristic peaks at 780 nm, indicating that ICG has been encapsulated into nanoparticles successfully. In addition, the quantitative analysis of IZH was performed, the drug loading capacity (DLC) of IZH was about 23.6 % by analysing the standard curve.

As shown in Fig. 2E, FT-IR spectra was also carried out to study the chemical structure of the products. A characteristic peak of the HA amides was also observed at 1625 cm^{-1}, 1576 cm^{-1}, and 1351 cm^{-1},

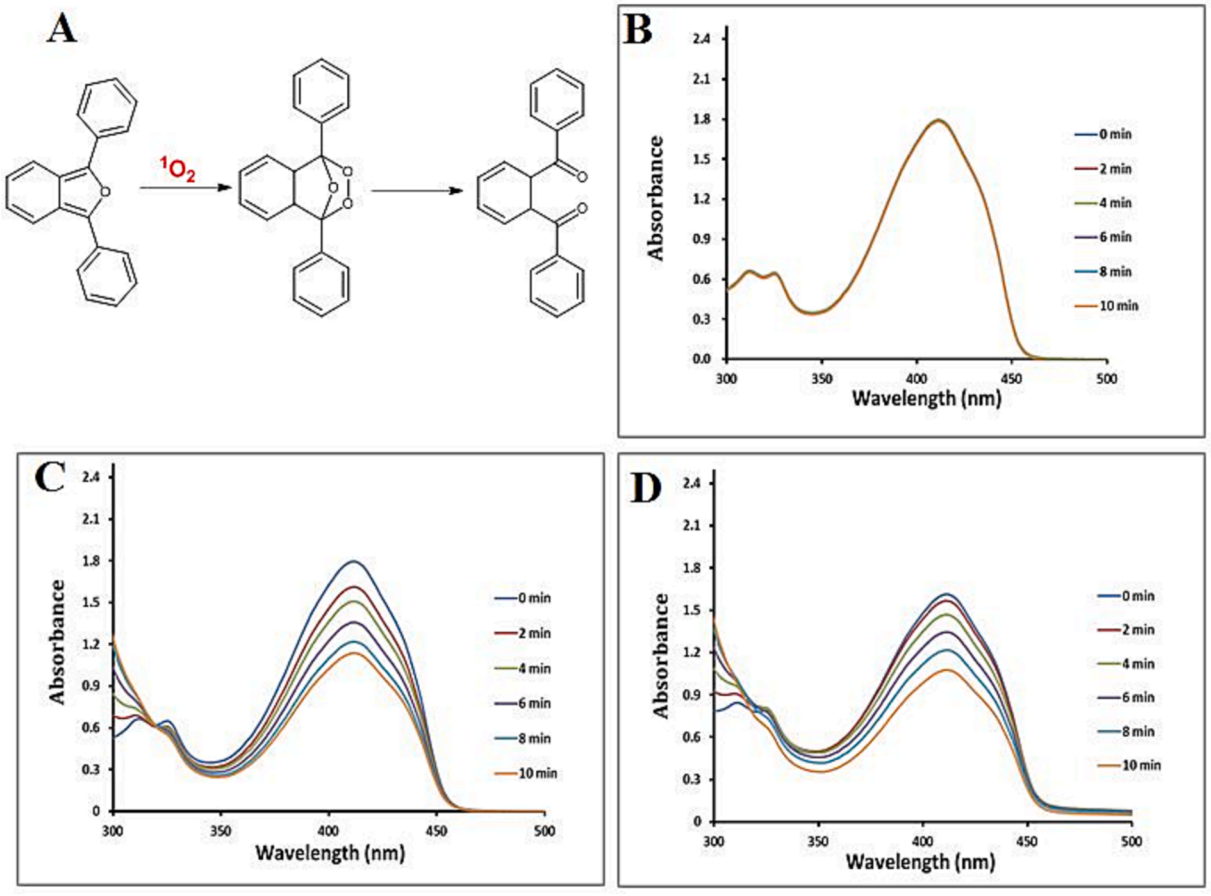

Fig. 4. (A) Reaction mechanism of DPBF oxidation by $^1O_2$. A spectrophotometric measurement determines ROS production. DPBF absorbance (B), and DPBF absorbance with ICG (C) or IZH (D), under irradiation with different time, respectively.

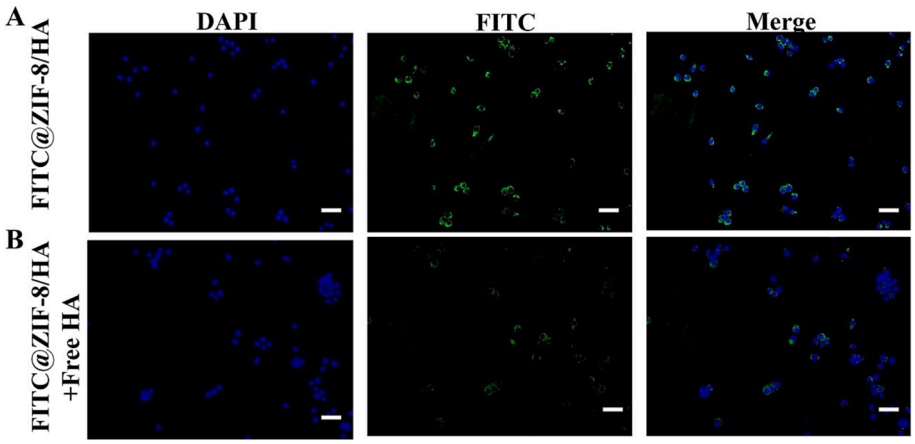

Fig. 5. Incubation of RAW 246.7 cells with FITC@ZIF-8/HA (A) and FITC@ZIF-8/HA pretreated with free-HA polymer (B) shown by fluorescence microscopy. Each image had a scale bar of 50 μm.

respectively, originating from the amide I and amide II and amide III bands at the spectrum of IZH (Alkrad et al., 2003). Moreover, Zn-N stretching was demonstrated in the spectrum of ICG@ZIF-8 by a peak at 421 cm^{-1} (Soltani et al., 2018). It is confirmed that IZH nanoparticles were synthesized successfully from these results.

The DLS method was used to monitor the change in zeta potential and size distribution of IZH over 6 days in order to investigate its storage stability. The zeta potential and average particle size of IZH did not change considerably as time progressed, as shown in Fig. 2F. It was confirmed that IZH has good stability, which is critical for the use of the drug as an antibacterial agent in clinical practice since it prevents abnormal release and inactivation.

3.2. pH-responsive drug release

As shown in Fig. 3, we conducted a controlled drug release test to determine the ICG release behavior from IZH. Incubated for 48 h in a neutral solution (pH 7.4), IZH had a lower release rate of drugs with an approximately 20 % release rate, indicating that IZH was stable in the normal physiological environment. The presence of this property can reduce the likelihood of unnecessary leakage of drugs during blood circulation. However, after incubation for 24 h at pH 5.5, 77.3 % of ICG was released from IZH, resulting from acidic environments that could break the coordination bonds between the metallic and organic active sites of ZIF-8(Zhang et al., 2022). It has been demonstrated that IZH particles are an effective pH-sensitive delivery system for releasing drugs into inflammatory sites, which has great therapeutic potential for intractable bacterial infections.

3.3. Measurement of reactive oxygen generation

In order to determine whether IZH was capable of generating reactive oxygen precisely, 1, 3-diphenylisobenzofuran (DPBF) was used as a singlet oxygen probe under NIR irradiation at 780 nm. An analytical reagent typically employed for ROS analysis, DPBF can react with $^1O_2$ quantitatively to produce an oxidation product (*o*-dibenzoylbenzene) that reduces DPBF's UV–vis absorption (Fig. 4A). As shown in Fig. 4B, in DMSO solutions containing DPBF, little evidence of DPBF reducing absorption was observed under laser irradiation. In comparison, DPBF's characteristic absorbance at 421 nm was clearly decreased in the presence of ICG (Fig. 4C) and IZH with an equivalent amount of ICG (Fig. 4D) after irradiation. These results suggested that IZH can be used for PDT treatment modality.

3.4. Intracellular uptake of IZH

As part of our investigation, we replaced the ICG in the nanostructure with FITC to determine whether HA is involved as a mediator of cell phagocytosis. FITC payloads in nanoparticles can be used as fluorescent markers to quantify FITC@ZIF-8/HA levels within intracellular compartments. As illustrated in Fig. 5, there was a great deal of brightness in the image of cells exposed to FITC@ZIF-8/HA without free HA, compared to cells exposed to FITC@ZIF-8/HA with free HA blocking CD44 receptors. The decreased fluorescent intensity was attributed to the interaction of free-HA with CD44 receptors, causing interference with the IZH's endocytosis mediated by CD44 receptors. According to the studies above, receptor-mediated endocytosis plays a critical role in macrophage internalization of IZH.

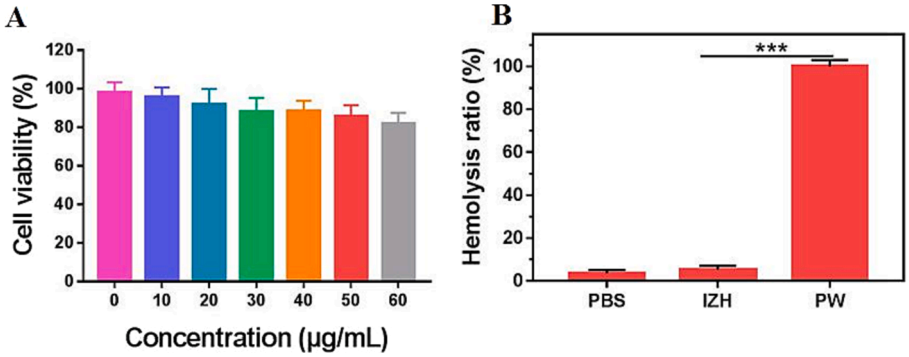

Fig. 6. (A) RAW 246.7 cell cytotoxicity *in vitro* at different concentrations of IZH; (B) IZH hemolysis on red blood cells. (For interpretation of the references to colour in this figure legend, the reader is referred to the web version of this article.)

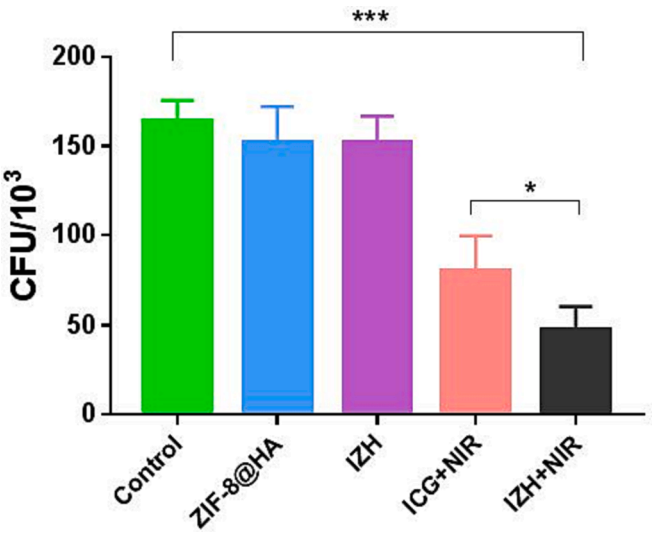

Fig. 7. RAW264.7 cells infected with MRSA were treated with PBS, ZIF-8@HA, IZH, ICG + NIR irradiation, IZH + NIR irradiation, respectively. The mean (SD) values of triplicate experiments are given. *p < 0.05, **p < 0.005, ***p < 0.001.

3.5. Biocompatibility of IZH in vitro

MTT cell viability tests were used to determine the cytotoxicity of IZH in the RAW 264.7 cells. As exhibited in Fig. 6A, the survivorship of RAW 264.7 cells still remained above 80 % even at a high concentration of 60 μg/mL, which indicated that the IZH had less toxicity for normal cells. In addition, a hemolysis assay was conducted in this study to determine IZH's blood compatibility. As shown in Fig. 6B, blood compatibility was excellent with 200 μg/mL concentration in IZH group at no obvious hemolysis of RBCs was detected. It was determined that IZH was safe enough to be applied to the organism which inspired us to investigate its use as a PDT therapy for treating infections *in vivo*.

3.6. Intracellular bacteria experiment

MRSA is one of the primary pathogens that is responsible for severe tissue infections, and the treatment of MRSA has become more challenging due to its ability to persist within phagocytic cells. We have already shown that IZH can eradicate intracellular bacteria *in vitro* in this study. MRSA-infected RAW 264.7 cells were treated with NIR radiation after being incubated with IZH. As displayed obviously in Fig. 7, Compared with the control group, ZIF-8@HA and IZH showed negligible inhibitory activity against intracellular bacteria. Additionally, the light treatment of the IZH group significantly inhibited the intracellular bacterial growth compared with the light treatment of the ICG group. It was evident that the IZH particles functionalized with HA significantly enhanced cellular uptake, allowing the antibacterial activity to be more pronounced against intracellular bacteria.

3.7. Therapeutic efficacy of IZH in vivo

Inspired by the outstanding antibacterial activity *in vitro*, further work was undertaken to investigate IZH's antibacterial properties *in vivo*. The bacterial pneumonia mouse models were divided into five groups and each group received different treatment according to the experimental design and the results were presented in the Fig. 8. Acute pneumonia mice treated with IZH + NIR, compared with those treated with control, ZIF-8@HA, IZH, or ICG + NIR, showed more effective suppression of MRSA (Fig. 8B). The better therapeutic effects might be attributed to the higher level of ICG in the lung tissues IZH + NIR treated mice than that in mice treated with ICG, which further verified the specific lung-targeting property of IZH. According to histopathological analyses, the alveoli tissue of control-treated, ZIF-8@HA-treated, and IZH-treated mice were seriously injured, with abundant inflammatory cells infiltrating compared to ICG + NIR-treated and IZH + NIR-treated group (Fig. 8C). As is notable, compared with the rest of the experiments, the lungs of the IZH under NIR irradiation-treated mice had significantly more complete alveoli. Taken together, the strategy may be useful for the development of new therapies for the treatment of

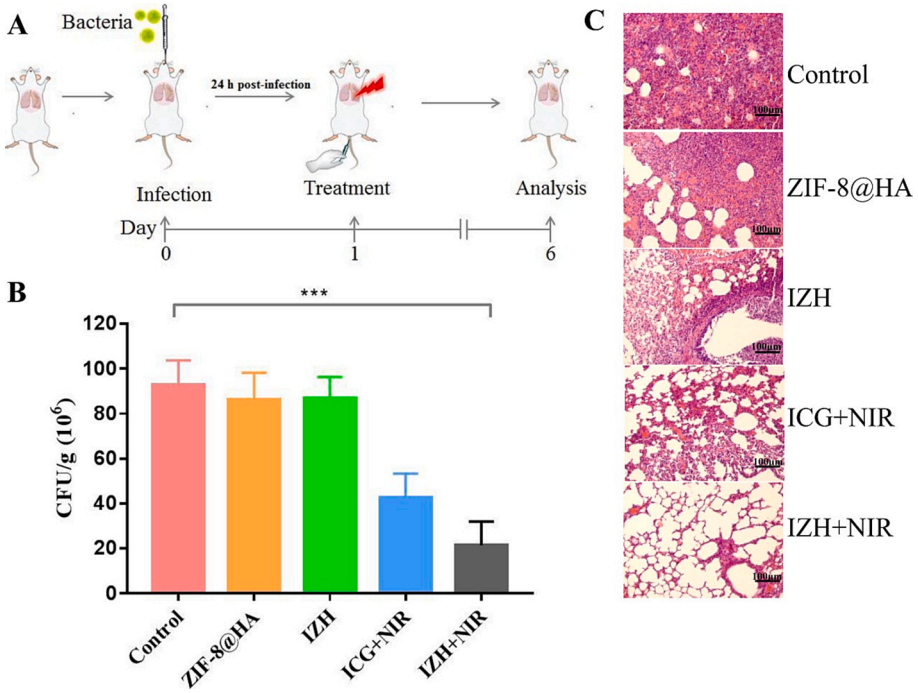

Fig. 8. (A) A schematic illustration of the construction and treatment of a pneumonia model; (B) In five animal groups, the mean number of CFU was recorded in lung tissue: PBS, ZIF-8@HA, IZH, ICG + NIR irradiation, IZH + NIR irradiation, respectively; (C) An analysis of the impact of five groups on lung tissues: PBS, ZIF-8@HA, IZH, ICG + NIR irradiation, IZH + NIR irradiation. The mean (SD) values of triplicate experiments are given. *p < 0.05, **p < 0.005, ***p < 0.001.

pneumonia caused by MRSA.

4. Conclusion

In summary, a novel drug-delivery system was developed for the treatment of pneumonia caused by methicillin-resistant *Staphylococcus aureus*. As the ICG was encapsulated into ZIF-8 NPs, coated with HA on the surface in order to achieve improved dispersibility and stability as well as enable infection site targeting. *In vitro* and *in vivo* evidence indicates that ICG@ZIF-8/HA nanoparticles have low systemic toxicity and excellent antibacterial performance. It demonstrates not only the development of the ZIF-8-based drug-delivery system but also the potential for bio-triggered nanotherapeutic design to improve the treatment of bacterial pneumonia, showing great promise for clinical translation.

Author contributions

Chunbo Lu conceived the experiments. Yujie Xu, Xiaoli Zhang, Congmin Niu, Shuyi Liang and Jiayi Guo carried out the experiments, performed data analysis. Chunbo Lu and Yujie Xu wrote and revised the manuscript. All authors approved the final version of the manuscript.

Declaration of competing interest

The authors declare that they have no known competing financial interests or personal relationships that could have appeared to influence the work reported in this paper.

Acknowledgments

This research was funded by the Natural Science Foundation of Shandong Province (Grant No. ZR2021QC178). The Authors are very grateful.

References

Alkrad, J.A., Mrestani, Y., Stroehl, D., Wartewig, S., Neubert, R., 2003. Characterization of enzymatically digested hyaluronic acid using NMR, Raman, IR, and UV-Vis spectroscopies. J. Pharm. Biomed. Anal. 31 (3), 545–550.

Chang, B., Qi, Y., Li, Y., Ning, G., 2021. Titanium carbide/zeolite imidazole framework-8/polylactic acid electrospun membrane for near-infrared regulated photothermal/photodynamic therapy of drug-resistant bacterial infections. J. Colloid Interface Sci. 599, 390–403.

Gajdács, M., 2019. The Continuing Threat of Methicillin-Resistant Staphylococcus aureus. Antibiotics (Basel, Switzerland) 8 (2), 52.

Gao, L., Chen, Q., Gong, T., Liu, J., Li, C., 2019. Recent advancement of imidazolate framework (ZIF-8) based nanoformulations for synergistic tumor therapy. Nanoscale 11 (44), 21030–21045.

Gardete, S., Tomasz, A., 2014. Mechanisms of vancomycin resistance in Staphylococcus aureus. J. Clin. Invest. 124 (7), 2836–2840.

Gerlach, D., Guo, Y., De Castro, C., Kim, S.H., Schlatterer, K., Xu, F.F., Pereira, C., Seeberger, P.H., Ali, S., Codée, J., Sirisarn, W., Schulte, B., Wolz, C., Larsen, J., Molinaro, A., Lee, B.L., Xia, G., Stehle, T., Peschel, A., 2018. Methicillin-resistant Staphylococcus aureus alters cell wall glycosylation to evade immunity. Nature 563 (7733), 705–709.

Hou, Z., Shankar, Y.V., Liu, Y., Ding, F., Subramanion, J.L., Ravikumar, V., Zamudio-Vázquez, R., Keogh, D., Lim, H., Tay, M., Bhattacharjya, S., Rice, S.A., Shi, J., Duan, H., Liu, X.W., Mu, Y., Tan, N.S., Tam, K.C., Pethe, K., Chan-Park, M.B., 2017. Nanoparticles of short cationic peptidopolysaccharide self-assembled by hydrogen bonding with antibacterial effect against multidrug-resistant bacteria. ACS Appl. Mater. Interfaces 9 (44), 38288–38303.

Hu, D., Deng, Y., Jia, F., Jin, Q., Ji, J., 2020. Surface charge switchable supramolecular nanocarriers for nitric oxide synergistic photodynamic eradication of biofilms. ACS Nano 14 (1), 347–359.

Lehar, S.M., Pillow, T., Xu, M., Staben, L., Kajihara, K.K., Vandlen, R., DePalatis, L., Raab, H., Hazenbos, W.L., Morisaki, J.H., Kim, J., Park, S., Darwish, M., Lee, B.C., Hernandez, H., Loyet, K.M., Lupardus, P., Fong, R., Yan, D., Chalouni, C., Mariathasan, S., 2015. Novel antibody-antibiotic conjugate eliminates intracellular S. aureus. Nature 527 (7578), 323–328.

Li, S., Cui, S., Yin, D., Zhu, Q., Ma, Y., Qian, Z., Gu, Y., 2017. Dual antibacterial activities of a chitosan-modified upconversion photodynamic therapy system against drug-resistant bacteria in deep tissue. Nanoscale 9 (11), 3912–3924.

Lu, C., Xiao, Y., Liu, Y., Sun, F., Qiu, Y., Mu, H., Duan, J., 2020. Hyaluronic acid-based levofloxacin nanomicelles for nitric oxide-triggered drug delivery to treat bacterial infections. Carbohydr. Polym. 229, 115479.

McGuinness, W.A., Malachowa, N., DeLeo, F.R., 2017. Vancomycin resistance in Staphylococcus aureus. Yale J. Biol. Med. 90 (2), 269–281.

Nannini, E., Murray, B.E., Arias, C.A., 2010. Resistance or decreased susceptibility to glycopeptides, daptomycin, and linezolid in methicillin-resistant Staphylococcus aureus. Curr. Opin. Pharmacol. 10 (5), 516–521.

Pérez, C., Zúñiga, T., Palavecino, C.E., 2021. Photodynamic therapy for treatment of Staphylococcus aureus infections. Photodiagn. Photodyn. Ther. 34, 102285.

Rehm, S.J., 2008. Staphylococcus aureus: the new adventures of a legendary pathogen. Cleve. Clin. J. Med. 75 (3), 177–192.

Ribeiro, I.P., Pinto, J.G., Souza, B., Miñán, A.G., Ferreira-Strixino, J., 2022. Antimicrobial photodynamic therapy with curcumin on methicillin-resistant Staphylococcus aureus biofilm. Photodiagn. Photodyn. Ther. 37, 102729.

Soltani, B., Nabipour, H., Nasab, N.A., 2018. Efficient storage of gentamicin in nanoscale zeolitic imidazolate framework-8 nanocarrier for pH-responsive drug release. J. Inorg. Organomet. Polym. 28, 1090–1097.

Stogios, P.J., Savchenko, A., 2020. Molecular mechanisms of vancomycin resistance. Protein Sci. : Publication Protein Soc. 29 (3), 654–669.

Thompson, R.E., Pardieck, J., Smith, L., Kenny, P., Crawford, L., Shoichet, M., Sakiyama-Elbert, S., 2018. Effect of hyaluronic acid hydrogels containing astrocyte-derived extracellular matrix and/or V2a interneurons on histologic outcomes following spinal cord injury. Biomaterials 162, 208–223.

Tian, H., Zhang, M., Jin, G., Jiang, Y., Luan, Y., 2021. Cu-MOF chemodynamic nanoplatform via modulating glutathione and H2O2 in tumor microenvironment for amplified cancer therapy. J. Colloid Interface Sci. 587, 358–366.

Tong, S.Y., Davis, J.S., Eichenberger, E., Holland, T.L., Fowler Jr, V.G., 2015. Staphylococcus aureus infections: epidemiology, pathophysiology, clinical manifestations, and management. Clin. Microbiol. Rev. 28 (3), 603–661.

Wang, X.H., Yu, Y.X., Cheng, K., Yang, W., Liu, Y.A., Peng, H.S., 2019. Polylysine modified conjugated polymer nanoparticles loaded with the singlet oxygen probe 1,3-diphenylisobenzofuran and the photosensitizer indocyanine green for use in fluorometric sensing and in photodynamic therapy. Mikrochim. Acta 186 (12), 842.

Xie, Z., Liang, S., Cai, X., Ding, B., Huang, S., Hou, Z., Ma, P., Cheng, Z., Lin, J., 2019. O2-Cu/ZIF-8@Ce6/ZIF-8@F127 composite as a tumor microenvironment-responsive nanoplatform with enhanced photo-/chemodynamic antitumor efficacy. ACS Appl. Mater. Interfaces 11 (35), 31671–31680.

Yan, X., Tarasi, S., Wang, S., Rostamizadeh, K., Hu, M., Morsali, A., Ramazani, A., Tarasi, R., Ahmadi, Y., 2023. Influence of pore structural properties in metal-organic frameworks on the host-guest interaction in drug delivery. Arab. J. Chem. 16 (8), 104887.

Yao, Q., Ye, Z., Sun, L., Jin, Y., Xu, Q., Yang, M., Wang, Y., Zhou, Y., Ji, J., Chen, H., Wang, B., 2017. Bacterial infection microenvironment-responsive enzymatically degradable multilayer films for multifunctional antibacterial properties. J. Mater. Chem. B 5 (43), 8532–8541.

Yuwen, L., Qiu, Q., Xiu, W., Yang, K., Li, Y., Xiao, H., Yang, W., Yang, D., Wang, L., 2021. Hyaluronidase-responsive phototheranostic nanoagents for fluorescence imaging and photothermal/photodynamic therapy of methicillin-resistant Staphylococcus aureus infections. Biomater. Sci. 9 (12), 4484–4495.

Zhang, Y., Lai, L., Liu, Y., Chen, B., Yao, J., Zheng, P., Pan, Q., Zhu, W., 2022. Biomineralized cascade enzyme-encapsulated ZIF-8 nanoparticles combined with antisense oligonucleotides for drug-resistant bacteria treatment. ACS Appl. Mater. Interfaces 14 (5), 6453–6464.

Zhang, X., Liu, L., Huang, L., Zhang, W., Wang, R., Yue, T., Sun, J., Li, G., Wang, J., 2019. The highly efficient elimination of intracellular bacteria via a metal organic framework (MOF)-based three-in-one delivery system. Nanoscale 11 (19), 9468–9477.

Zhang, S., Ye, J., Liu, X., Wang, G., Qi, Y., Wang, T., Song, Y., Li, Y., Ning, G., 2022. Dual stimuli-responsive smart fibrous membranes for efficient photothermal/photodynamic/chemo-therapy of drug-resistant bacterial infection. Chem. Eng. J. 432, 134351.

Zhao, Y., Yu, C., Yu, Y., Wei, X., Duan, X., Dai, X., Zhang, X., 2019. Bioinspired heteromultivalent ligand-decorated nanotherapeutic for enhanced photothermal and photodynamic therapy of antibiotic-resistant bacterial pneumonia. ACS Appl. Mater. Interfaces 11 (43), 39648–39661.

Zhao, Y., Wang, H., Zou, X., Wang, D., Fan, Y., Zhao, X., Li, M., Yang, L., Liang, C., 2022. Antibacterial vancomycin@ZIF-8 loaded PVA nanofiber membrane for infected bone repair. Int. J. Mol. Sci. 23 (10), 5629.

Żywicka, A., Fijałkowski, K., Junka, A.F., Grzesiak, J., El Fray, M., 2018. Modification of bacterial cellulose with quaternary ammonium compounds based on fatty acids and amino acids and the effect on antimicrobial activity. Biomacromolecules 19 (5), 1528–1538.